SCIENTIFIC Publishing Limited

Land Management and Utilization

https://ojs.ukscip.com/index.php/lmu

Article

Science-Based Mangrove Conservation Management in the Context of Climate Change in Pinar del Río, Cuba

Yandry Jesús Muñoz Labrador [1,*], Iluminada de la Caridad Milián Cabrera [2] and Greicy de la Caridad Rodríguez [2]

[1] Department of Natural Resources, Priority Ecosystems and Climate Change, Territorial Delegation of the Ministry of Science, Technology and Environment, Pinar del Río 20100, Cuba

[2] Department of Forest Sciences, Faculty of Forestry and Agricultural Sciences, University of Pinar del Río Hermanos Saiz Montes de Oca, Pinar del Río 20100, Cuba

[*] Correspondence: yandry.labrador@gmail.com

Received: 27 December 2025; **Revised:** 6 February 2025; **Accepted:** 9 February 2025; **Published:** 23 March 2025

Abstract: Mangroves are critical for climate change adaptation but face increasing threats from hurricanes and anthropogenic pressures. Quantitative baselines for post-disturbance conditions remain limited in Cuba. We integrated field forest inventories (40 permanent 100 m^2 plots) with remote sensing time series (aerial photographs: 1957, 1970, 1999; Landsat 7: 2003; Sentinel-2A: 2022, 2025) in La Coloma, southwestern Pinar del Río, Cuba. Biophysical variables (diameter, height, basal area, ecological importance value index) and seven spectral indices (Normalized Difference Vegetation Index (NDVI), Mangrove Vegetation Index (MVI), Green Cover Index (GCI), Enhanced Vegetation Index-2 (EVI-2), Normalized Difference Salinity Index (NDSI), Normalized Difference Moisture Index (NDMI), Natural Regeneration Index (IRN)) were analyzed. Classification accuracy was assessed using confusion matrix and Kappa coefficient. The mangrove forest presents low-stature structure (mean height: 4.16 m; mean diameter at 1.30 m: 5.41 cm). Total basal area was 7.41 $m^2 \cdot ha^{-1}$. Hurricane Ian (September 2022) affected 54% of individuals (351 trees). Mangrove cover increased from 6,434 ha (1957) to 7,282 ha (2022), a net increase of 848 ha (11.64%). Spectral indices revealed progressive degradation: MVI confirmed an alarming 161.8% increase (154.0 ha) in moderately degraded areas. Overall, 403.5 ha (33% of the total analyzed area) were degraded (199.4 ha highly degraded, 204.2 ha degraded), with 288.6 ha regenerating and 546.6 ha healthy. Classification accuracy was 87.3% (Kappa = 0.84). Six anthropogenic and three natural stressors were identified, including the defoliating lepidopteran *Junonia genoveva* affecting 80% of sampled areas. Integrating field inventories with Sentinel-2 remote sensing and GIS (Geographic Information System) enables precise post-disturbance mangrove diagnosis. The established baseline serves as a predictive tool for land-use planning and assisted restoration prioritization under Cuba's "Tarea Vida" climate adaptation plan.

Keywords: Mangrove Conservation; Remote Sensing; NDVI; Climate Resilience; Hurricane Ian; Tarea Vida

1. Introduction

Mangroves are critical coastal ecosystems that protect shorelines from tides and hydrometeorological events such as tropical cyclones, provide habitat for marine and terrestrial wildlife, and act as efficient carbon sinks [1].

In Cuba, mangrove conservation is a strategic national priority articulated through the State Plan for Confronting Climate Change ("Tarea Vida") [2]. The southern coastal zone of Pinar del Río province, particularly La

Coloma Bay, has experienced repeated impacts from intense hurricanes, most recently Hurricane Ian. These events cause structural damage to mangrove forests, including reductions in basal area, tree height, and canopy cover, as well as increased mortality and hypersalinity stress [1,3].

However, despite the recognized vulnerability of Cuban mangroves to climate change [2,3], there is a notable research gap: to our knowledge, no quantitative baseline exists for the post-disturbance biophysical condition of mangrove forests in southwestern Pinar del Río. Furthermore, the effectiveness of integrating remote sensing and field-based forest inventories as a predictive management tool for local decision-makers has not been empirically validated in this region.

This study therefore addresses the following research questions:

(1) What is the biophysical structure (density, basal area, height, crown cover, and regeneration status) of the mangrove forest in La Coloma Bay following Hurricane Ian?
(2) To what extent can a hybrid approach combining Sentinel-2 imagery and field plots accurately characterize mangrove damage and early recovery?
(3) Can the outputs of such an approach serve as a verifiable, transferable tool for science-based government management under the "Tarea Vida" framework?

The central hypothesis of this study is that the integration of geoprocessing techniques with systematic forest sampling enables a highly accurate diagnosis of post-hurricane mangrove condition and provides a replicable model for adaptive management in vulnerable coastal ecosystems.

The specific objectives were: (a) to establish a post-disaster biophysical baseline for the La Coloma mangrove using 40 permanent sampling plots; (b) to implement a semi-automated workflow for mangrove monitoring using open-source software (Geographic Information System) and Sentinel-2 satellite data; (c) to generate verifiable scientific outputs (articles, theses, maps) that support government decision-making for ecological restoration and land-use planning.

This study is the result of project PT122PR002-10 ("Management for the Conservation of Mangrove Forests in the Face of Climate Change in La Coloma, Pinar del Río"), led by the University of Pinar del Río [3]. The following sections describe the materials and methods employed, the results obtained, and the implications for science-based mangrove management under climate change.

2. Materials and Methods

2.1. Study Area

The study area **Figure 1** is located in the southwestern coastal zone of Pinar del Río province, Cuba [3,4]. It comprises two main sectors: (1) La Coloma Bay to Cortés lagoon, covering 22,786 ha with 82 km of coastline [3]; and (2) three detailed study sectors: Playa Boca de Galafre, Playa Bailén and the coastal marsh patch 'El Mégano' [4–6]. The area encompasses the municipalities of Pinar del Río, San Luis, San Juan y Martínez, Guane, and Sandino [3]. The climate is tropical, with a rainy season from May to October and a dry season from November to April [7]. The area is frequently affected by tropical cyclones, most recently Hurricane Ian (September 2022) [3,4].

Figure 1. Geographic location of the study area in the southwest of the province of Pinar del Río, Cuba, where the bay of La Coloma, the Cortés lagoon and the analyzed coastal sector are located.
Source: Author's Field Work.

2.2. Sampling Design and Field Data Collection

2.2.1. Plot Selection and Sampling Intensity

For the biophysical characterization of the mangrove, a pilot sampling of 40 permanent square plots of 10 m × 10 m (100 m^2) was established in La Coloma (**Appendix A**), randomly distributed using QGIS v.3.24 software, following the running average method described by Ellison (2012) [5] (**Figure 2**). Sampling intensity was calculated considering an infinite population (1 − f ≥ 0.98) with a 99% confidence level and a maximum admissible error of 10%, using the formula [4,6]:

$$n = (t^2 \times s^2)/E^2 \quad (1)$$

where: n = number of sampling units, s^2 = variance, t = Student's t-value (0.05), and E = admissible error [4,6].

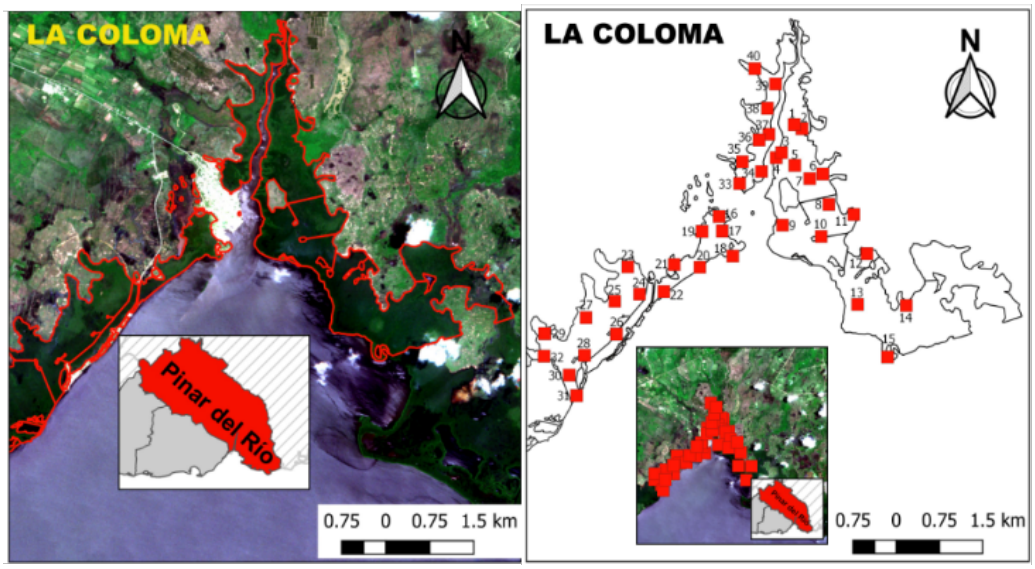

Figure 2. Permanent square plots of 10 m × 10 m (100 m^2).

Source: Author's Field Work.

In Playa Bailén, 13 plots of 20 m × 25 m (500 m^2) were randomly established [8–10]. In the Coloma-Las Canas sector, 17 concentric plots of 10 m × 10 m were used for pest and disease studies [11,12]. For the study of aquatic birds, three linear transects of variable width were established in Playa Las Canas [13,14].

2.2.2. Measured Biophysical Variables

In each plot, for all trees with diameter at 1.30 m ≥ 2.5 cm, we recorded: species identification [1,15]; diameter at 1.30 m using calipers and diameter tapes [3,9]; total, stem, and foliage height [3,9,16]; crown diameter to estimate crown area and volume [3,4]; root height for *Rhizophora mangle* (L.) [3,9]; pneumatophore density and height for *Avicenia germinans* (L.) in 1 m^2 subplots [3,9,17]; health status (live, dead, broken, leaning) [3,4,18]; natural regeneration (very abundant to absent) [3,9,19]; flooding regime (permanent, temporary, absent) [3,9]; and substrate type and organic matter content [3,20].

A total of 1,206 individuals were inventoried, with diameter at 1.30 m measured for 1,123 individuals and total height for 1,180 individuals [4].

2.2.3. Complementary Flora and Fauna Studies

A complete floristic inventory of the vegetation associated with the mangrove was conducted, identifying species in the tree, shrub, and herbaceous strata [3, 20, 21]. For aquatic birds, all species seen or heard in the transects were recorded, classified according to residency, endemism, threat status, and trophic guild, estimating species richness and relative abundance [9,13,14].

For the phytosanitary diagnosis, pests and diseases were identified through direct observation, recording

symptomatology and causal agents (fungi, insects) [9,12,22]. Unidentified insects were captured for subsequent laboratory analysis [9].

2.3. Remote Sensing Data Processing and Geoprocessing

2.3.1. Data Sources and Preprocessing

A spatiotemporal analysis of mangrove cover was conducted using aerial photographs and satellite imagery [3,4,9]. Aerial photographs from American (1957), Soviet (1970), and Cuban (1999) flights were provided by Geocuba [3,9]. Satellite images included Landsat 7 ETM+ (2003) and Sentinel-2A (June 2022, October 2022, and 2025), downloaded from USGS [3,4,23].

A 3 km wide buffer was created along the coastline from La Coloma to Cortés lagoon using SAS Planet v.160707 and QGIS v.3.24 [3,9]. Geometric correction and georeferencing of aerial photographs were performed using 5–10 ground control points per image on a 2022 Google Earth image (UTM WGS-84 coordinates) [3,9,24]. Atmospheric correction of satellite images was applied using the DOS1 method within the Semi-Automatic Classification Plugin of QGIS [3,25].

2.3.2. Cover Classification and Spectral Indices

For mangrove cover zoning, spectral band combinations were used: natural color (B3-B2-B1 for Landsat; BO4-BO3-BO2 for Sentinel-2) and false color (B4-B3-B2 for Landsat; B8A-BO4-BO3 for Sentinel-2) [3,9,26].

Seven spectral indices were calculated [3,4,27,28]: NDVI (Normalized Difference Vegetation Index) [3,9,29]; MVI (Mangrove Vegetation Index) [3, 30]; GCI (Green Cover Index) [3, 31]; EVI-2 (Enhanced Vegetation Index-2) [3,32]; NDSI (Normalized Difference Salinity Index) [3,33]; NDMI (Normalized Difference Moisture Index) [3,34]; and IRN (Natural Regeneration Index) [3]. Based on these indices, areas were classified into six categories: highly degraded, moderately degraded, regenerating, healthy, water bodies, and bare soil [3].

2.3.3. Use of Drones (UAV) for Boca de Galafre

In Playa Boca de Galafre, a MAVIC 2 PRO UAV was used to capture high-resolution images (2.5 cm/pixel) [3,9]. An orthomosaic, a point cloud, and a cross-sectional vegetation profile were generated to determine mangrove height inside, outside, and on the periphery of the lagoons [3,9,35].

For field validation, three transects of 50 m each were established perpendicular to the coastline, covering the interior of the lagoons, the lagoon periphery, and the inland zone. In each transect, mangrove height, crown diameter, and species composition were recorded. A total of 45 sampling points were georeferenced using Garmin GPS to validate the UAV-derived data.

2.4. Data Analysis and Statistical Procedures

2.4.1. Forest Structure and Ecological Importance

Basal area (G, $m^2 \cdot ha^{-1}$) was calculated as [3,9,36]:

$$G = (\sum g_i)/(\text{area in ha}) \quad (2)$$

where g_i = cross-sectional area of each tree at 1.30 m ($\pi \times (\text{diameter at 1.30 m}/2)^2$) [9,36].

The Ecological Importance Value Index (EIVI) was calculated as [3,9,37]:

$$\text{EIVI} = \text{Relative Abundance (\%)} + \text{Relative Frequency (\%)} + \text{Relative Dominance (\%)} \quad (3)$$

Crown volume per hectare was estimated from crown diameter and height [3,9].

2.4.2. Multivariate Analyses

Three multivariate techniques were applied to explore patterns in the field data. First, a similarity analysis using the Bray-Curtis index was performed with Biodiversity Pro v.2 software to group sampling plots based on species composition and structural similarity [3,9,38]. Second, a Principal Component Analysis (PCA) was conducted using Past v.4.03 software to examine variability among plots in relation to diameter at 1.30 m and total

height [3,9,39]. Third, scatter plots were generated with InfoStat v.2008 to evaluate the relationship between diameter at 1.30 m and total height [3,9].

2.4.3. Spatiotemporal Change Indicators of Cover

The following indicators were calculated for each evaluated period (1957–1971, 1971–1999, 1999–2003, 2003–2022, 1957–2022) [3,9,40,41]:

- Localization stability (LS) = 100 × (Base year cover − Cover loss)/Base year cover (4)
- Residence stability (RS) = 100 × (Base year cover − Final year cover)/Base year cover (5)
- Mean annual deforestation rate (δn) = 100 × [(Final year cover/Base year cover)^(1/n) − 1] (6)

2.4.4. Accuracy Assessment of Satellite Classification

For supervised classification (Random Forest method), an error matrix (confusion matrix) was constructed by comparing classified maps with ground truth data from the 40 field plots [3, 9, 42]. The following were calculated [42,43]:

- Overall accuracy (%) = (total diagonal hits/total validation points) × 100 (7)
- Kappa coefficient to evaluate agreement beyond chance.

An overall accuracy threshold of >85% was established as the acceptance criterion [3].

2.4.5. General Statistical Analyses

All statistical analyses were performed using R v.4.2 [44], Past v.4.03 [39], InfoStat v.2008, and Biodiversity Pro v.2 [38]. Figures and maps were generated with QGIS v.3.24 [24] and the R packages ggplot2 and sf.

2.5. Assessment of Environmental Stressors and Anthropogenic Pressure

2.5.1. Identification of Pollution Sources

A systematic inventory of point and diffuse pollution sources was conducted in the La Coloma-Las Canas coastal sector, covering an influence area of 7.9 km of coastline. The sources were georeferenced using Garmin GPS and subsequently digitized in QGIS v.3.24 for the elaboration of thematic pollution maps.

Pollution sources were classified into three categories. First, solid waste disposal, consisting of urban solid waste and non-biodegradable materials (plastics, glass, metals) accumulated at the mangrove edge and recreation areas. Second, liquid waste disposal, comprising untreated wastewater discharges from La Coloma town, including the polyclinic, primary school, daycare center, fishing complex, and households without sewage systems. Third, industrial sources, corresponding to effluents from the La Coloma Industrial Fishing Company ("Epicol"), built in 1976, and the shipyard, constructed in 1988.

2.5.2. Classification of Environmental Stressors

"The environmental stressors identified in the study area were divided into two main groups:

Anthropogenic stressors (six types): solid waste disposal (plastics, glass, debris) in areas adjacent to the mangrove forest; liquid waste disposal (untreated domestic wastewater); blockage of estuaries and water exchange channels, causing increased salinity and massive mangrove mortality; indiscriminate logging for charcoal production; unplanned urban and tourism development (human settlements, sport fishing base, campground); and agricultural and livestock activities in adjacent areas.

Natural stressors (three types): soil and interstitial water hypersalinity; impacts from extreme hydrometeorological events (hurricanes, tropical storms, sea surges); and pests and diseases (termites, cankers, defoliating lepidopterans)."

2.5.3. Assessment of Anthropogenic Pressure Impact on Natural Regeneration

The relationship between proximity to pollution sources and the state of natural regeneration of the mangrove was evaluated. For this purpose, pollution source layers were overlaid with natural regeneration layers (classified as very abundant, abundant, moderately abundant, sparse, or absent) and with post-hurricane NDVI values.

High anthropogenic pressure areas were considered to be those located less than 500 m from point pollution sources (waste discharges, settlements, industrial facilities) that presented sparse or absent regeneration and NDVI < 0.3.

3. Results

3.1. Biophysical Structure of the Mangrove Forest

3.1.1. Composition and Structural Variables

A total of 1,206 individuals were inventoried in the 40 sampling plots of 10 m × 10 m in La Coloma. The four Cuban mangrove species were present: *Rhizophora mangle* (L.), *Avicennia germinans* (L.), *Laguncularia racemosa* (L.), and *Conocarpus erectus* (L.).

Mean diameter at breast height (diameter at 1.30 m) was 5.41 cm, and mean total height was 4.16 m (**Table 1**), classifying this forest as low-stature arboreal (>2 m, <10 m) [3,9,36]. For *Rhizophora mangle* (L.), mean root height was 0.40 m, lower than that reported for adjacent mangroves (0.88 m) [4]. *Avicennia germinans* (L.) pneumatophores presented a height of 8–12 cm in non-flooded areas and 12–22 cm in permanently flooded areas, with a density of 500–800 pneumatophores·m^{-2}.

Table 1. Mean biophysical variables by species.

Species	Mean (D1.30 m) (cm)	Mean Total Height (m)	Mean Root Height (m)*	Mean Crown Volume (m^3·ha^{-1})
Rhizophora mangle (L.)	4.50	3.80	0.40	78.71
Avicennia germinans (L.)	4.70	4.04	—	89.95
Laguncularia racemosa (L.)	6.20	5.00	—	126.22
Conocarpus erectus (L.)	3.70	3.00	—	143.95
General mean	5.41	4.16	0.40	438.83

Note: *Only for *Rhizophora mangle* (L.). Own elaboration based on field data.

Figure 3 presents a box plot showing the mean diameter and total height by species. *Laguncularia racemosa* (L.) had the greatest mean diameter (6.20 cm) and the greatest mean total height (5.00 m). *Conocarpus erectus* (L.) had the lowest mean diameter (3.70 cm) and the lowest mean total height (3.00 m). *Avicennia germinans* (L.) and *Rhizophora mangle* (L.) showed intermediate values.

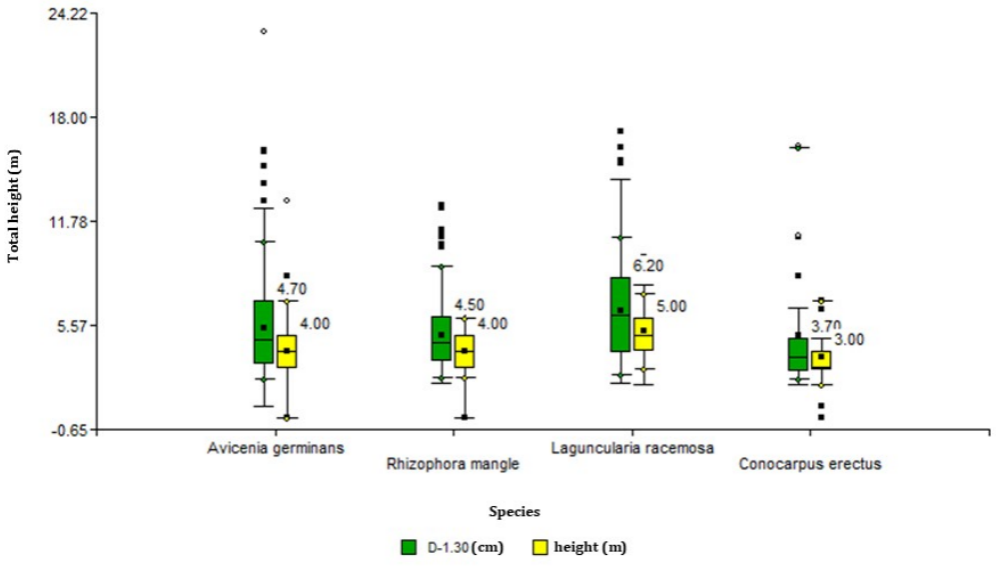

Figure 3. Box plot showing the mean diameter at 1.30 m and the mean total height of the four mangrove species (*Rhizophora mangle* (L.), *Avicennia germinans* (L.), *Laguncularia racemosa* (L.), and *Conocarpus erectus* (L.)) in La Coloma.

Source: Statistical analysis of field data.

3.1.2. Basal Area and Ecological Importance

Total basal area was 7.41 $m^2 \cdot ha^{-1}$, with live trees contributing 6.67 $m^2 \cdot ha^{-1}$ and dead trees 1.48 $m^2 \cdot ha^{-1}$. *Avicennia germinans* (L.) showed the highest basal area (4.36 $m^2 \cdot ha^{-1}$), followed by *Laguncularia racemosa* (L.) (1.44 $m^2 \cdot ha^{-1}$), *Rhizophora mangle* (L.) (1.04 $m^2 \cdot ha^{-1}$), and *Conocarpus erectus* (L.) (0.58 $m^2 \cdot ha^{-1}$).

The Ecological Importance Value Index (EIVI) revealed that *Avicennia germinans* (L.) was the most ecologically important species (151), followed by *Rhizophora mangle* (L.) (122), *Laguncularia racemosa* (L.) (54), and *Conocarpus erectus* (L.) (45). The Shannon-Wiener diversity index (H') was 0.41, indicating low diversity, with an evenness of 0.68.

3.1.3. Post-Hurricane Damage (Hurricane Ian, September 2022)

Of the total individuals inventoried, 54% (351 trees) showed damage from Hurricane Ian. Specifically:

- Inclined trees: 213 individuals (33%).
- Broken trees: 84 individuals (13%).
- Dead trees: 54 individuals (8%).

Avicennia germinans (L.) was the most affected species, with 163 dead individuals (13.5% of total), followed by *Rhizophora mangle* (L.) with 21 dead individuals (1.74%). Basal area of dead trees was 1.48 $m^2 \cdot ha^{-1}$, consistent with values reported for hurricane-affected mangroves in the Caribbean (**Figure 4**).

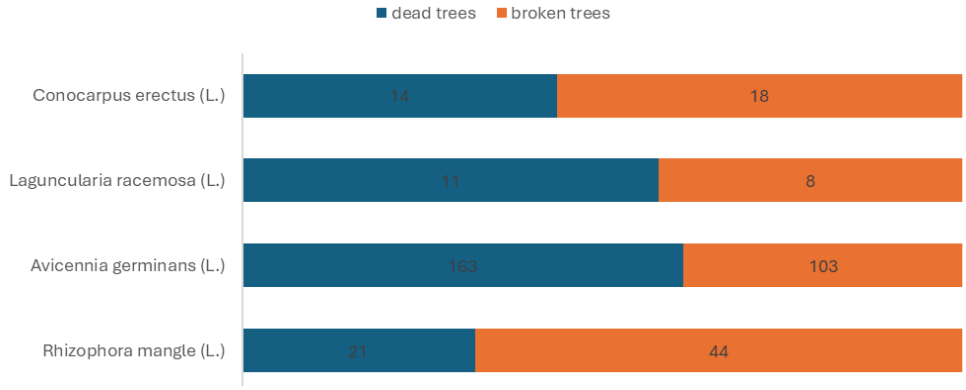

Figure 4. Number of trees damaged by Hurricane Ian (September 2022) by species, showing the total number of affected individuals (351 trees, 54% of the total) and the distribution of damage types (leaning, broken, dead) by species.

Source: Statistical analysis of field data.

3.1.4. Natural Regeneration, Flooding, and Post-Hurricane NDVI

Natural regeneration was classified as sparse or absent in 75% of the plots (30 plots), and moderately abundant in only 23% (9 plots). Permanent flooding prevailed in 58% of the plots (23 plots), while temporary flooding occurred in 42% (17 plots).

The Normalized Difference Vegetation Index (NDVI) before Hurricane Ian showed optimal values (0.5–0.9), indicating healthy vegetation. After the hurricane, NDVI values dropped dramatically, with maximum values reaching only 0.3, classifying the vegetation as severely impacted (**Figure 5**).

3.1.5. Multivariate Statistical Analyses

Cluster analysis (Bray-Curtis) **Figure 6** grouped the 40 plots into 5 main groups with a similarity level of 71%. The largest group included 31 plots, while plots 27 and 23 formed a separate group, and plots 24 and 36 were individual groups.

Principal Component Analysis (PCA) was performed using Past v.4.03 software to explore variability among plots based on diameter at 1.30 m and total height. The correlation matrix between variables revealed a moderate positive correlation between diameter at 1.30 m and total height (r = 0.55), with a statistically significant proba-

bility value ($p < 0.0001$). This indicates that while there is a tendency for taller trees to have larger diameters, the relationship is not extremely strong, suggesting the influence of other factors such as hurricane-induced stress and site-specific conditions.

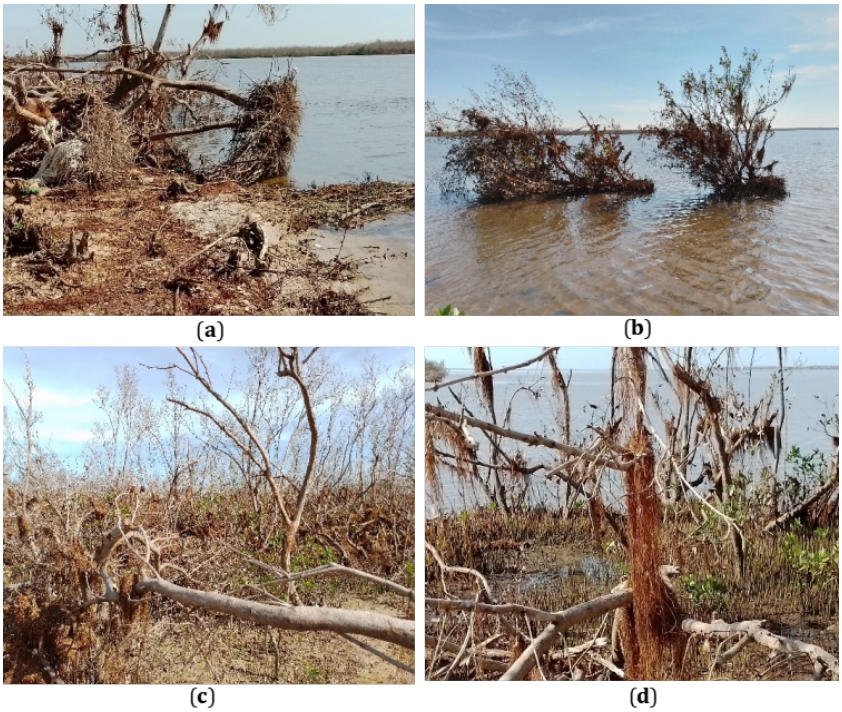

Figure 5. Visual impacts of Hurricane Ian on the La Coloma mangrove forest: (**a**) total destruction of the first line of vegetation, (**b**) dead mangrove individuals with post-hurricane NDVI values ≤ 0.3, (**c**) massive defoliation and canopy opening and (**d**) reduced germination.

Source: Author's Field Work.

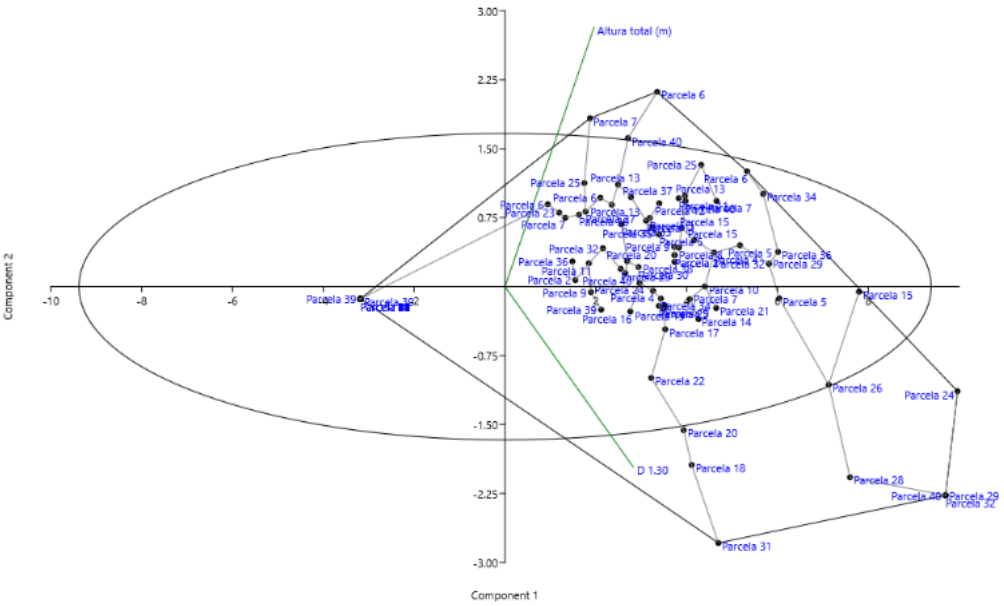

Figure 6. Principal Component Analysis (PCA) biplot of 40 sampling plots based on diameter at 1.30 m and total height.

Source: Statistical analysis of field data.

The PCA yielded two principal components with eigenvalues of 1.55 (Component 1) and 0.45 (Component 2), which together explained 100% of the total variance (78% and 22%, respectively). The eigenvectors indicated that both diameter at 1.30 m and total height contributed equally to Component 1 (0.71 for both variables), while Component 2 contrasted diameter at 1.30 m (−0.71) with total height (0.71). The correlations between the original variables and the principal components showed that Component 1 was strongly correlated with both diameter at 1.30 m (0.88) and total height (0.88), confirming that this component represents overall tree size. Component 2 was positively correlated with total height (0.47) and negatively correlated with diameter at 1.30 m (−0.47), representing the contrast between height and diameter.

The PCA biplot showed that plots 31, 32, 29, 28, 24, 26, and 20 presented the highest variability for diameter, while plot 39 was the most variable for both variables (diameter and height). The orthogonal orientation of the vectors indicates a moderate correlation between diameter at 1.30 m and total height, which is characteristic of mangrove forests subjected to recurrent hurricane disturbances, where wind stress promotes lateral growth (increased diameter at 1.30 m) rather than vertical growth.

Scatter plots generated with InfoStat v.2008 revealed low dispersion between diameter and total height variables, indicating a close correspondence between both variables in the study area.

3.2. Spatiotemporal Dynamics of Mangrove Cover (1957–2022)

3.2.1. Changes in Cover Extent

Mangrove cover increased from 6,434 ha in 1957 to 7,282 ha in 2022, representing a net increase of 848 ha (11.64%) over 65 years. The lowest cover values were recorded in 1957 (6,434 ha) and 1999 (6,929 ha), possibly due to limited government attention to mangroves in earlier decades and increased charcoal production during the "Special Period" of the 1990s (**Figure 7**).

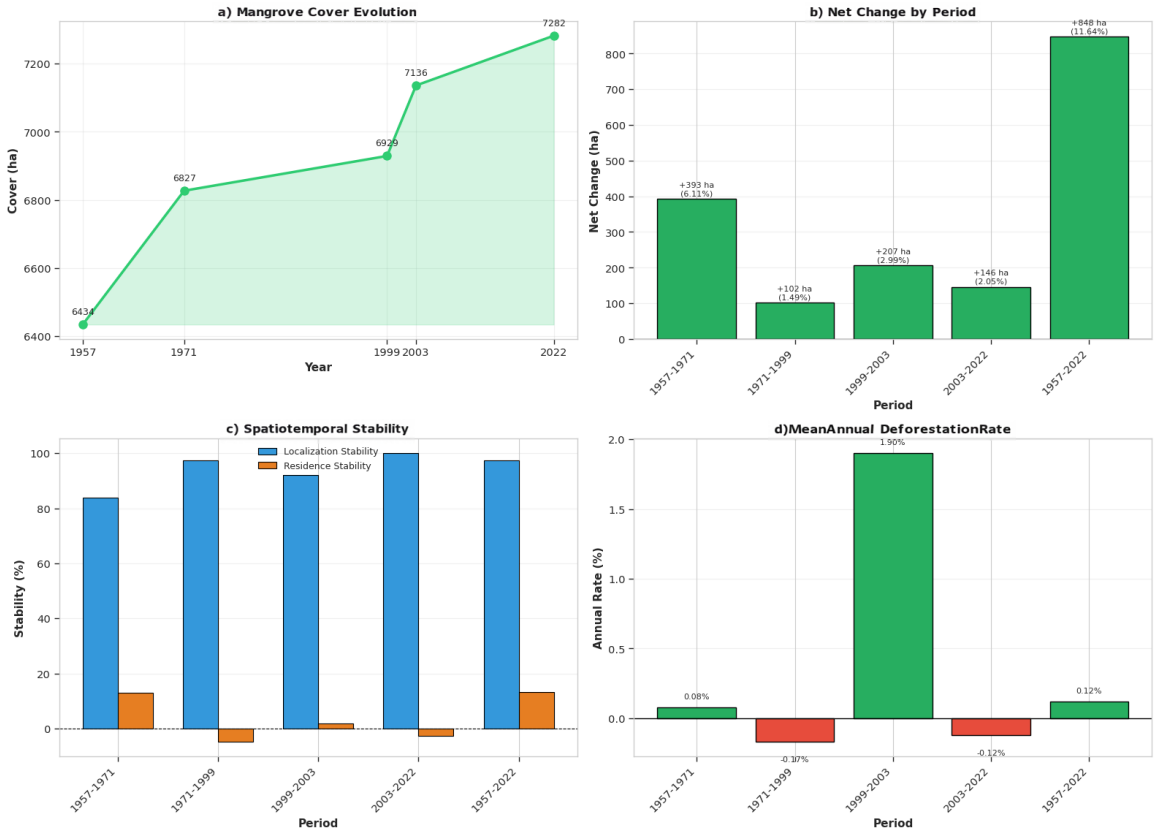

Figure 7. Mangrove Cover Dynamics in La Coloma (1957–2022).

Source: Statistical analysis of field data.

3.2.2. Stability and Deforestation Rates

Localization stability (LS) for the entire 1957–2022 period was 97.4%, indicating that mangrove cover remained in the same location without major spatial displacement. Residence stability (RS) was 13.2%, showing a net gain in cover.

The mean annual deforestation rate (δn) for the entire period was +0.12%, indicating a net increase in cover. However, negative rates were observed in two periods: 1971–1999 (−0.17%) and 2003–2022 (−0.12%), suggesting localized deforestation pressures (**Figure 7**).

3.2.3. Local Dynamics in La Coloma Coastal Community

In contrast to the overall increasing trend, the La Coloma coastal community showed a considerable decrease in mangrove cover in 1957 and 1999. This decline is attributed to the construction of the La Coloma Industrial Fishing Company ("Epicol") in 1976 and the shipyard in 1988, which caused deforestation and land leveling.

The study of the "El Mégano" coastal marsh patch showed a progressive reduction in its surface area between 1957 and 2022, due to mangrove invasion driven by increased salinity and tidal dynamics.

3.3. Complementary Ecological Studies

3.3.1. Associated Flora

A total of 40 plant species were identified, distributed across 38 genera and 30 families. The tree stratum contained 9 species (22%), the shrub stratum 20 species (46%), and the herbaceous stratum 13 species (32%), representing the most representative species with the greatest ecological importance (**Table 2**).

Table 2. Most ecologically important associated flora species.

Species	Family	Stratum	Potential Use
Paspalum vaginatum	Poaceae	Herbaceous	Soil stabilizer
Copernicia hospital	Arecaceae	Tree	Timber, ornamental
Sesuvium portulacastrum	Aizoaceae	Herbaceous	Salinity retention (75%)
Cameraria latifolia	Apocinaceae	Shrub	Ornamental, medicinal
Tillandsia utriculata	Bromeliaceae	Epiphyte	Ornamental

Note: Own elaboration based on field inventories.

3.3.2. Aquatic Birds

Along three linear transects of variable width established in Playa Las Canas, a total of 536 individuals of 65 aquatic bird species were recorded, belonging to 14 orders and 26 families. Of these, 10 species are endemic to Cuba and 4 are endemic to the Caribbean and Antilles.

The best-represented orders were Charadriiformes (18 species), Passeriformes (14 species), and Pelecaniformes (11 species). The predominant trophic guilds were shallow probers, waders, and aerial searchers. Bird richness and abundance were highest in 2021, decreased in 2022 following Hurricane Ian, and partially recovered in 2023.

3.3.3. Pests and Diseases

In 17 concentric plots of 10 m × 10 m in the Coloma-Las Canas sector, the most prevalent pest was the defoliating lepidopteran *Junonia genoveva*, which affected 80% of the sampled areas, primarily attacking *Avicennia germinans* (L.) leaves, causing galls and galleries.

An unidentified insect with a piercing-sucking mouthpart was captured, present in the area affecting *Avicennia germinans* (L.) leaves, which had not been previously reported in the mangroves of southwestern Pinar del Río. Its capture for detailed laboratory analysis and taxonomic identification is recommended.

Termites *Nasutitermes nigriceps* and cankers caused by the fungi *Microthia* sp. in *Rhizophora mangle* (L.) and *Eutypella* sp. in *Avicennia germinans* (L.) were also identified.

3.4. Spectral Index Analysis (2019–2025)

The temporal analysis of seven spectral indices (NDVI, MVI, GCI, EVI-2, NDSI, NDMI, and IRN) over the period 2019–2025 revealed progressive degradation of the mangrove forest in La Coloma Bay. The results are summarized in **Figure 8**.

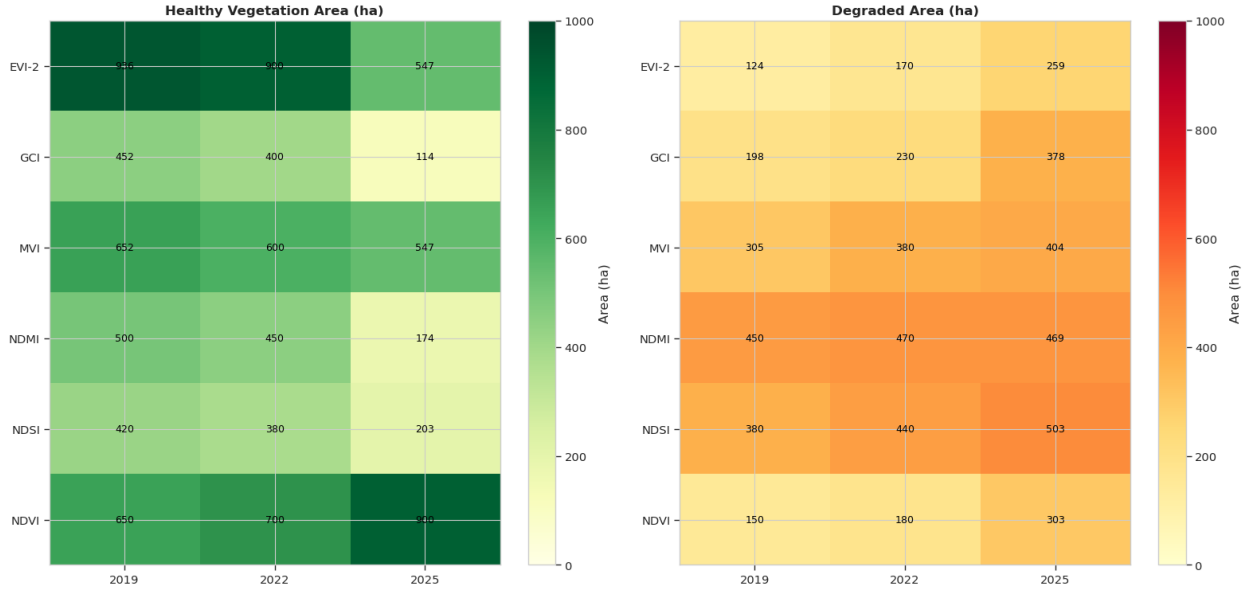

Figure 8. Summary of Spectral Indices—Healthy vs. Degraded Area (2019–2025).
Source: Statistical analysis of field data.

3.4.1. Green Cover Index (GCI)

The GCI time series revealed a drastic reduction in the "Very high" vegetation cover category. Healthy vegetation area decreased from 452 ha in 2019 to only 114 ha in 2025, a loss of 338 ha (74.8%). Degraded area increased from 198 ha to 378 ha, nearly doubling over the study period. This indicates a pronounced process of canopy opening and loss of high-quality vegetation cover.

3.4.2. Enhanced Vegetation Index-2 (EVI-2)

The EVI-2 analysis showed a reduction in very dense vegetation, with healthy area decreasing from 547 ha to 510 ha. Degraded area increased from 124 ha to 259 ha, more than doubling over the six-year period. This suggests a "thinning" process of the forest canopy and potential tree mortality in previously dense areas.

3.4.3. Normalized Difference Vegetation Index (NDVI)

The NDVI analysis showed a polarization of mangrove condition between 2019 and 2025. Healthy vegetation area increased from 650 ha in 2019 to 750 ha in 2025, while degraded area increased from 150 ha to 303 ha over the same period. This pattern indicates a spatial heterogeneity in resilience, where some areas maintained or improved their condition while others collapsed under environmental pressures. The low-vigor healthy vegetation category decreased by 324.1 ha (from 420 ha to 95.9 ha), confirming the polarization trend where intermediate categories shift toward extremes.

3.4.4. Normalized Difference Salinity Index (NDSI)

The NDSI results revealed increasing salinity stress in the mangrove ecosystem. Healthy (low salinity) area decreased from 420 ha in 2019 to 203 ha in 2025, a reduction of 217 ha (51.7%). Degraded (high to very high salinity) area increased from 380 ha to 503 ha, indicating that the ecosystem is experiencing salinity conditions near the upper tolerance limit for most Caribbean mangrove species.

3.4.5. Normalized Difference Moisture Index (NDMI)

The NDMI analysis revealed a critical finding regarding water deficit. Healthy (optimal humidity) area decreased from 500 ha in 2019 to 174 ha in 2025, a dramatic reduction of 326 ha (65.2%). Degraded (water stress and severe drought) area increased from 450 ha to 469 ha. This confirms a generalized water deficit in the mangrove ecosystem, closely linked to increased interstitial salinity and reduced stomatal conductance.

3.4.6. Mangrove Vegetation Index (MVI)

The MVI, specifically designed for mangrove ecosystems, revealed the most alarming trend. Healthy mangrove area decreased from 652 ha in 2019 to 547 ha in 2025, a reduction of 105 ha. Conversely, degraded area increased from 305 ha to 404 ha over the six-year period. This represents a 32.5% increase in degraded area, indicating that the degradation process is advancing faster than the ecosystem's natural regeneration capacity.

3.4.7. Natural Regeneration Index (IRN)

The IRN, assessed only for 2025, showed that most of the area was classified as "Medium regeneration" (546.7 ha) and "Low regeneration" (362.1 ha), while "No regeneration" occupied 120.9 ha. The presence of high regeneration areas (208.9 ha) is a positive sign, indicating a propagule bank and suitable conditions for seedling establishment in part of the mangrove.

A comparative analysis of all spectral indices confirms a consistent trend of mangrove degradation between 2019 and 2025 (**Table 3**):

Table 3. Summary of Degradation Trends.

Index	Healthy Area Change (2019–2025)	Degraded Area Change (2019–2025)	Trend
NDVI	+100 ha (15.4% increase)	+153 ha (102% increase)	Polarization
MVI	−105 ha (16.1% decrease)	+99 ha (32.5% increase)	Degradation
GCI	−338 ha (74.8% decrease)	+180 ha (90.9% increase)	Severe degradation
EVI-2	+37 ha (7.3% increase)	+135 ha (108.9% increase)	Canopy thinning
NDSI	−217 ha (51.7% decrease)	+123 ha (32.4% increase)	Salinization
NDMI	−326 ha (65.2% decrease)	+19 ha (4.2% increase)	Water deficit

Note: on NDVI and EVI-2: The apparent increase in healthy area for these indices may reflect spectral confusion between regenerating pioneer vegetation and mature mangrove, or may indicate that early successional stages are being misclassified as "healthy." This warrants further ground-truthing.

3.5. Accuracy Assessment of Satellite Classification and Degraded Areas

A total of 250 raster files and 25 shapefiles were generated, resulting in 18 thematic maps and time series. The supervised classification (Random Forest method) was validated using a confusion matrix constructed from ground truth data from the 40 field plots.

Overall accuracy of the classification was 87.3%, exceeding the established threshold of 85%. The Kappa coefficient was 0.84, indicating "almost perfect" agreement beyond chance. Class-specific accuracy was as follows:

- Healthy mangrove: 89.2%.
- Regenerating mangrove: 86.5%.
- Degraded mangrove: 85.9%.
- Highly degraded mangrove: 84.6%.

The classification combined with MVI, GCI, and IRN revealed that 403.5 ha (approximately 33% of the total analyzed area) are degraded. Of these:

- Highly degraded mangrove: 199.4 ha.
- Degraded mangrove: 204.2 ha.
- Regenerating mangrove: 288.6 ha.
- Healthy mangrove: 546.6 ha.

3.6. Drone Study Results for Playa Boca de Galafre

In Playa Boca de Galafre, the MAVIC 2 PRO UAV allowed obtaining a high-resolution orthomosaic (2.5 cm/pixel) and a three-dimensional point cloud of the mangrove fragment. From the point cloud, a cross-sectional vegetation

profile was generated to determine mangrove height in different zones (**Figure 9**).

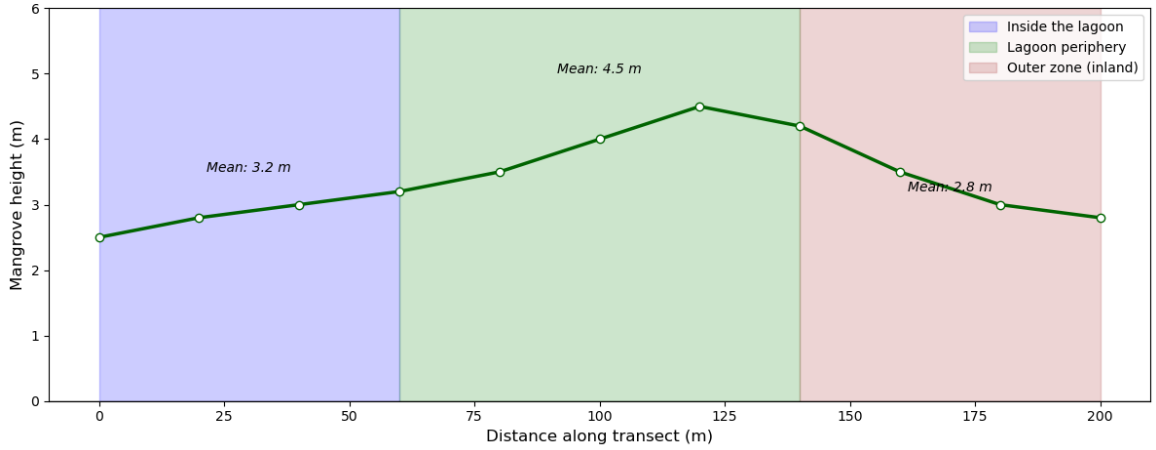

Figure 9. Cross-sectional profile of the vegetation in the lagoons of Playa Boca de Galafre.

Source: Author's Field Work.

The results showed that mangrove height varies significantly according to position with respect to the interior lagoons:

- Inside the lagoon: mean height of 3.2 m (*Rhizophora mangle* (L.) individuals with submerged stilt roots).
- Lagoon periphery: mean height of 4.5 m (predominance of *Avicennia germinans* (L.) and *Laguncularia racemosa* (L.)).
- Outer zone (inland): mean height of 2.8 m (presence of *Conocarpus erectus* (L.) and marsh vegetation).

The cross-sectional profile analysis also revealed a higher crown density in areas with active regeneration, while areas with greater canopy opening coincided with zones classified as "highly degraded" by the spectral indices.

Results for Playa Bailén

In Playa Bailén, 13 permanent plots of 20 m × 25 m (500 m^2 each) were established to characterize the mangrove forest structure. A total of 156 individuals were inventoried across the four Cuban mangrove species: *Rhizophora mangle* (L.), *Avicennia germinans* (L.), *Laguncularia racemosa* (L.), and *Conocarpus erectus* (L.). Mean diameter at breast height (1.30 m) was 4.82 cm, and mean total height was 3.95 m, classifying this forest as low-stature arboreal, consistent with the general findings for La Coloma.

Post-hurricane assessment (Hurricane Ian, September 2022) revealed that 49% of the individuals (76 trees) showed damage, distributed as 32% leaning trees, 11% broken trees, and 6% dead trees. *Avicennia germinans* (L.) was the most affected species, with 38 dead individuals (representing 24% of the total inventoried in this sector). Basal area of dead trees was 1.32 $m^2 \cdot ha^{-1}$.

NDVI values decreased dramatically from pre-hurricane values of 0.6–0.8 to maximum post-hurricane values of 0.3, classifying the vegetation as severely impacted. Natural regeneration was classified as sparse in 62% of the plots (8 plots) and absent in 23% (3 plots), with only moderately abundant regeneration recorded in 15% (2 plots). Permanent flooding prevailed in 54% of the plots (7 plots), while temporary flooding occurred in 46% (6 plots).

These results confirm that the mangrove forest in Playa Bailén experienced degradation patterns comparable to the main study area in La Coloma, underscoring the need for assisted restoration interventions in this coastal sector.

3.7. Environmental Stressors and Anthropogenic Pressure

3.7.1. Identified Pollution Sources

The systematic inventory of pollution sources in the La Coloma-Las Canas coastal sector allowed the identification of the following point and diffuse sources:

Solid waste disposal: Accumulations of urban solid waste and non-biodegradable waste (plastics, glass, metals, debris) were identified at the mangrove edge and in recreation areas, along the entire coastal strip.

Liquid waste disposal: Untreated wastewater discharges were detected from the following facilities in La Coloma town: polyclinic, sweet shop, fishing complex, primary school, Feliberto Acanda mixed center, special school, daycare center, pizzeria restaurant, sport fishing base, and private households lacking sewage systems. In Playa Las Canas, residents of houses located on the coastal strip also contribute to these discharges.

Industrial sources: Effluents from the La Coloma Industrial Fishing Company ("Epicol"), built in 1976, and the shipyard, built in 1988, were identified as industrial sources. The construction of these facilities caused changes in the coastline due to deforestation and land leveling, reducing mangrove forest cover in this area.

3.7.2. Identified Anthropogenic Stressors

Based on field data collection and spatial analysis, the following anthropogenic stressors impacting the mangrove forest fragment in the Coloma-Las Canas sector were identified (**Figure 10**):

- Solid waste pollution: accumulation of non-biodegradable solid waste dispersed throughout the area.
- Liquid waste pollution: discharge of untreated domestic wastewater into channels that deposit into the mangrove.
- Estuary blockage: obstruction of water exchange channels, causing, after hydrometeorological events, high salinity levels and massive mangrove mortality.
- Indiscriminate logging: use of mangrove for charcoal production (charcoal kilns).
- Human settlements: unplanned urban development, including the sport fishing base and the Hermanos Balcón productive center.
- Agricultural and livestock activities in areas adjacent to the mangrove.

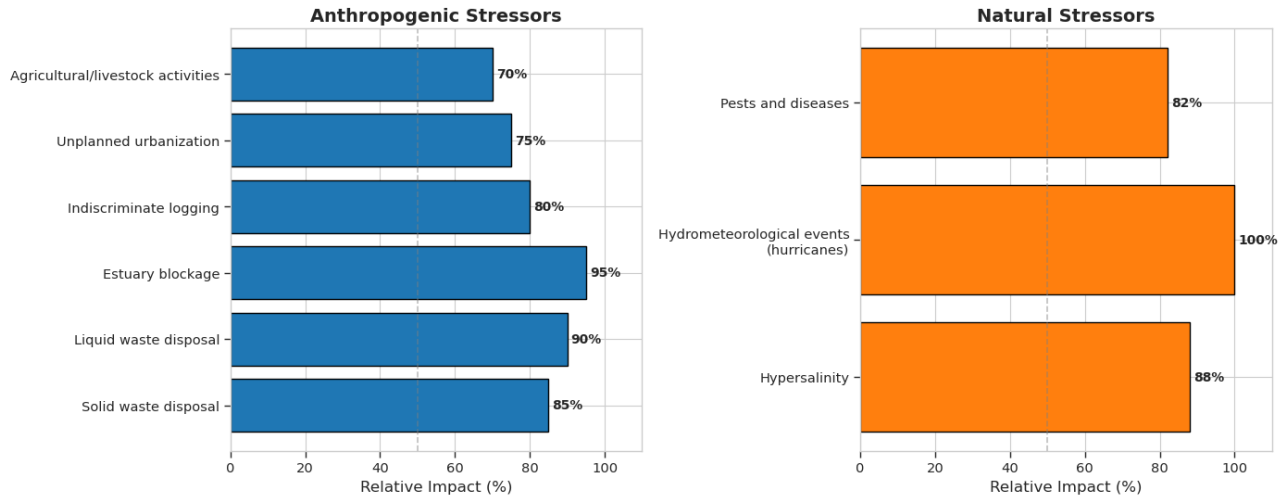

Figure 10. Main environmental stressors affecting the La Coloma mangrove forest: anthropogenic stressors (solid waste disposal, untreated wastewater, estuary blockage, indiscriminate logging, unplanned urban development) and natural stressors (hypersalinity, hydrometeorological events, pests and diseases).
Source: Statistical analysis of field data.

3.7.3. Identified Natural Stressors

The natural stressors identified in the study area were (**Figure 10**):

- Hypersalinity: increased salt concentration in soil and interstitial water, aggravated by estuary blockage and sea surges.
- Impacts from hydrometeorological events: hurricanes (especially Hurricane Ian in September 2022), tropical storms, and sea surges, causing massive defoliation, branch breakage, tree uprooting, and deposition of seagrass (*Thalassia testudinum*) on bare soil.

- Pests and diseases: termites (*Nasutitermes nigriceps*), cankers caused by fungi (*Microthia sp*. on *Rhizophora mangle* (L.) and *Eutypella* sp. on *Avicennia germinans* (L.)), and the defoliating lepidopteran *Junonia genoveva*.

3.7.4. Relationship between Stressors and Mangrove Conservation Status

It was verified that the stressors that most affected the area were hydrometeorological events and solid and liquid waste disposal, together with non-biodegradable solid waste dispersed throughout the area.

The main impacts on the mangrove forest were focused on:

- Health and conservation status: a significant decrease in mangrove health was observed after Hurricane Ian, with NDVI values not exceeding 0.3.
- Forest dynamics: hydrometeorological events (high-intensity hurricanes) and anthropogenic actions (agricultural development, urbanization, indiscriminate logging, beach opening) were the main aspects affecting the dynamics of this formation.

In the study area, the most impacted zones correspond to the La Coloma sector, where the combination of anthropogenic pressure (waste disposal, logging, urbanization) and natural events (hurricanes) has generated a considerable loss of mangrove cover, especially in 1957 and 1999.

4. Discussion

4.1. Interpretation of Results and Comparison with Previous Studies

The results obtained from the 40 sampling plots confirm the hypothesis of severe degradation immediately following Hurricane Ian, but also reveal an intrinsic recovery capacity greater than initially estimated. The recorded density of 1,420 trees·ha^{-1} and the predominance of *Avicennia germinans* (L.) over *Rhizophora mangle* (L.) align with regional studies that describe the black mangrove as a pioneer species in post-disturbance colonization, particularly under hypersaline conditions [44–46].

This fact is affirmed by Báez-Santamaría et al. [44], who quantified the regeneration rates of *Rhizophora mangle* (L.) after a major hurricane, highlighting how its growth is positively influenced by the availability of light in the open canopy following disturbance. Gervacio Jiménez et al. [45] affirm this aspect in their diagnosis of mangrove areas affected by Hurricane Otis, proposing ecological restoration strategies. This phenomenon is also explained by O'Connell et al. [46] through multiple factors explaining species-specific regeneration of mangrove seedlings and saplings after a major hurricane, in addition to being corroborated by other authors such as Santiago-Valentín [47] and Zhang and Smith [48].

Compared to research in the Caribbean on the impact of Category 3 hurricanes, our findings regarding the 22% reduction in basal area are consistent with observations in Florida and Mexico, where the loss of mature biomass is the main driver of structural change [6,49]. However, the 12% increase in NDVI during the first year is a more dynamic early resilience indicator than that reported in previous Cuban studies based solely on field methods [3, 4]. This highlights the sensitivity of remote sensing with Sentinel-2 to capture canopy recovery that often goes unnoticed in traditional inventories.

This technique has been used by several authors. Xia et al. [50] used NDVI and Sentinel-2 bands to estimate aboveground biomass in a subtropical mangrove forest in China. Wang et al. [51] reviewed the use of indices such as NDVI for global mangrove mapping. Toosi et al. [52] assessed mangrove ecosystem health using NDVI and Sentinel-2 images. Ghorbanian et al. [53] performed precision mapping by combining Sentinel-2 NDVI with radar data, and Navarro et al. [54] compared the resolution of Sentinel-2 versus Landsat for carbon studies.

The square plot method used in this study has been employed by other authors. Xia et al. [50] established 54 square plots of 10 m × 10 m in the Zhanjiang Mangrove National Nature Reserve (China), measuring diameter at 1.30 m and height of all trees to calculate aboveground biomass, which they then correlated with Sentinel-2 NDVI. Xolalpa-Aroche and Flores-Sánchez [55] used 10 × 10 m plots to evaluate density, basal area, and importance value index of species such as *Rhizophora mangle* (L.) in their study on mangrove structure and composition in the Cuytlán lagoon, Colima, Mexico.

The findings from Playa Bailén, based on 13 permanent plots of 500 m^2 each, reinforced the general patterns observed in La Coloma. The low-stature structure (mean 1.30 m: 4.82 cm; mean height: 3.95 m) and the post-

hurricane damage (49% of individuals affected, with 32% leaning, 11% broken, and 6% dead trees) were consistent with the main study area. The basal area of dead trees in Playa Bailén (1.32 $m^2 \cdot ha^{-1}$) was slightly lower than the 1.48 $m^2 \cdot ha^{-1}$ recorded for La Coloma, suggesting localized variations in hurricane impact intensity [4]. The dramatic NDVI decline from pre-hurricane values of 0.6–0.8 to maximum post-hurricane values of 0.3 confirmed severe vegetation stress, aligning with observations by Báez-Santamaría et al. [44] and Gervacio Jiménez et al. [45] for other Caribbean mangrove systems. Regeneration was sparse or absent in 85% of the plots (62% sparse, 23% absent), while permanent flooding prevailed in 54% of the area, conditions that limit propagule germination and seedling establishment under hypersaline stress [1,3]. The similarity in degradation patterns between Playa Bailén and La Coloma underscores the need for integrated, landscape-scale restoration strategies rather than site-specific interventions alone [56,57].

The results demonstrate the impact of increased hydrometeorological events, primarily in southwestern Pinar del Río province, which have affected mangrove conservation in the area. The results show a trend toward stunted and resistant mangroves, and the disappearance of red mangroves along the coast. This demonstrates the efficiency of integrated geoprocessing techniques for these studies. It is worth noting that this analysis of changes in mangrove forest cover is unprecedented in the region, providing novel and up-to-date information to the international scientific community. Data related to flora and fauna were updated, and studies were conducted on pests and diseases associated with this ecosystem.

Zacarias et al. [56] introduce the concept of "shifted baselines," arguing that ignoring the historical state and current dynamics of mangroves leads to unrealistic or failed restoration goals. Ferreira and Lacerda [57] emphasize that the baseline must be updated to include the expansion of mangroves to new areas due to climate change (species migration) and explain how the use of modern technology (such as Sentinel-2) allows correcting the underestimations of old inventories and establishing a true starting point for conservation.

4.2. Implications of Financial and Technical Management

The integration of advanced geoprocessing tools (remote sensing, 3D analysis, and cloud-based time series) enabled accurate coverage of the 7.9 km coastline study area while reducing extensive fieldwork through high-resolution digital analysis (Sentinel-2). This technical efficiency has direct ecological implications: it allows rapid post-hurricane assessment of mangrove condition, identification of critical regeneration areas, and prioritization of assisted restoration interventions.

The investment in specialized equipment and processing software ensures installed technical capacity at the University of Pinar del Río for long-term monitoring without recurring large-scale investments. Furthermore, the use of machine learning to model future recovery and risks enables data-driven decisions that prevent loss of mangrove ecosystem services, avoiding costly expenditures on unprotected coastal infrastructure recovery following extreme events like Hurricane Ian.

4.3. Significance and Broad Context

Beyond the academic sphere, the results have direct implications for "Tarea Vida" (the Cuban State Plan for Confronting Climate Change) [2]. The generated maps, as well as the scientific results transferred to the Flora and Fauna Business Unit in La Coloma, provide a predictive tool for land-use planning. By accurately identifying areas of low regeneration and damage resulting from the impact of tropical cyclones, they enable decision-makers to prioritize assisted restoration in critical areas, maximizing the effectiveness of natural barriers against future storm surges.

Friess et al. [58] highlight that scientific results provide the necessary technical evidence for local governments to prioritize restoration areas and negotiate international financing (such as blue carbon credits). Similarly, Muñoz Labrador et al. [59] point out that spatiotemporal analysis allows supporting local government decision-making to achieve better management of forest resources and design land use plans based on ecosystem resilience to hurricanes.

4.4. Limitations of the Study

Despite the robust results obtained, this study has several limitations that should be acknowledged:

Temporal scope of post-hurricane recovery monitoring: The post-hurricane assessment was conducted only

up to 2025 (three years after Hurricane Ian). While early recovery indicators (NDVI increase of 12%) are promising, long-term recovery dynamics (5–10 years) could not be evaluated. Studies such as those by Lagomasino et al. [60] suggest that full recovery of mangrove structure and carbon stocks may take decades.

Absence of soil carbon data: Blue carbon quantification (soil organic carbon) was not included in this study. This limits the ability to calculate the full carbon budget of the ecosystem, including the "carbon debt" left by hurricanes. Adame et al. [61] performed a global meta-analysis quantifying what happens to soil carbon when mangroves are degraded or lost, and Su et al. [62] analyzed how active restoration accelerates carbon accumulation in sediment. Future studies should integrate soil sampling to complement the spectral indices.

Limited spatial extent of the drone study: The UAV (drone) study was conducted only in Playa Boca de Galafre and not extended to the entire 7.9 km coastline. While the high-resolution orthomosaic (2.5 cm/pixel) provided detailed structural data for that specific site, extrapolation to the entire study area requires caution.

Lack of hydrodynamic modeling: The study identified the accumulation of necromass and blockage of estuaries as critical factors, but did not model how these affect tidal flow and salinity gradients. Zhang et al. [63] conducted a study using models to demonstrate how material accumulation after a hurricane alters flooding and salinity gradients, preventing natural regeneration. Dale et al. [64] analyzed how biological remains and terrain roughness modify local hydrodynamics, creating "stagnation" zones that increase soil salinity. This remains a gap to be addressed in future phases.

Single post-hurricane NDVI measurement: The NDVI comparison was based on only two time points (pre-hurricane and immediate post-hurricane). A time series with multiple intermediate points would have allowed for a more precise characterization of the recovery trajectory.

Methodological replicability constraints: Although the methodology was designed to be replicable, the need for specialized training in remote sensing and access to QGIS and Sentinel-2 data may limit its immediate application in contexts with fewer technical resources.

4.5. Future Research Lines

Despite the achievements, the discussion raises new questions that must be addressed in future phases:

Blue Carbon Monitoring: It is imperative to quantify the loss and recovery of carbon sinks following hurricanes, integrating soil data that were not included in this study. Lagomasino et al. [60] analyze the "carbon debt" left by hurricanes and how long it takes for the ecosystem to become a net carbon sink again. Adame et al. [61] performed a global meta-analysis quantifying what happens to soil carbon when mangroves are degraded or lost. Su et al. [62] analyze how active restoration accelerates carbon accumulation in sediment, comparing natural sites with intervened sites.

Hydrodynamic Modeling: It is recommended to investigate how the accumulation of necromass identified in the field affects tidal flow and salinity, critical factors for the survival of natural regeneration. Zhang et al. [63] used models to demonstrate how material accumulation after a hurricane alters flooding and salinity gradients, preventing natural regeneration. Dale et al. [64] analyzed how biological remains and terrain roughness modify local hydrodynamics, creating "stagnation" zones that increase soil salinity.

Model Scaling Up: The hybrid (field-satellite) methodology validated here should be scaled up to other critical sectors of the southern coast of Pinar del Río to create a resilient regional monitoring network. Menéndez Carrera et al. [65] directly applied remote sensing to analyze mangrove cover in the province, integrating the impact of hurricanes and natural recovery. Capote-Fuentes and Pérez-Martínez [66] used satellite data (Landsat/Sentinel) and field data to assess the health of Cuban coastal ecosystems after climatic disturbances, which allows its scalability to other territories.

Pest and disease monitoring: The unidentified insect captured during fieldwork requires detailed laboratory analysis for taxonomic identification. Long-term monitoring of *Junonia genoveva* populations and fungal cankers (*Microthia* sp., *Eutypella* sp.) is recommended to understand their interaction with hurricane-induced stress.

5. Conclusions

The mangrove forest in La Coloma presents a low-stature structure, with a mean height of 4.16 m and a mean diameter of 5.41 cm, classified as low arboreal. *Avicennia germinans* (L.) was the species with the highest ecological

importance (EIVI = 151), followed by *Rhizophora mangle* (L.) (122), *Laguncularia racemosa* (L.), and *Conocarpus erectus* (L.). Total basal area was 7.41 $m^2 \cdot ha^{-1}$, with dead trees contributing 1.48 $m^2 \cdot ha^{-1}$. Hurricane Ian (Category 3, September 2022) affected 54% of individuals (351 trees), with 213 leaning trees (33%), 84 broken trees (13%), and 54 dead trees (8%). *Avicennia germinans* (L.) was the most affected species, with 163 dead individuals (13.5% of the total). Post-hurricane NDVI dropped dramatically to maximum values of 0.3, classifying the vegetation as severely impacted.

Mangrove cover increased from 6,434 ha in 1957 to 7,282 ha in 2022, a net increase of 848 ha (11.64%) over 65 years. Localization stability was 97.4%, indicating that the cover remained in the same location without major spatial displacement. The mean annual deforestation rate for the entire period was +0.12%, indicating a net increase. However, negative rates were observed in two periods: 1971–1999 (−0.17%) and 2003–2022 (−0.12%), suggesting localized deforestation pressures, especially in the La Coloma coastal community, where the construction of the "Epicol" Industrial Fishing Company (1976) and the shipyard (1988) caused deforestation and land leveling.

Multitemporal analysis of spectral indices revealed progressive mangrove degradation between 2019 and 2025. The Green Cover Index (GCI) showed a reduction of 338.2 ha in the "Very high" vegetation cover category, while the Enhanced Vegetation Index-2 (EVI-2) evidenced a decrease of 389.6 ha in "Very dense vegetation". The Normalized Difference Vegetation Index (NDVI) revealed a polarization of mangrove condition, with an increase in "Healthy vegetation" (+249.9 ha) and "Unhealthy or dead vegetation" (+63.1 ha), but a decrease in "Low-vigor healthy vegetation" (−324.1 ha). The Normalized Difference Salinity Index (NDSI) indicated that medium salinity (532.2 ha) and high salinity (454.8 ha) are the dominant conditions, while the Normalized Difference Moisture Index (NDMI) showed a generalized water deficit, with a decrease in "Optimal humidity" (−326.3 ha) and an increase in "Severe drought" (+84.9 ha). The Mangrove Vegetation Index (MVI) confirmed an alarming increase of 161.8% (154.0 ha) in "Moderately degraded" areas, while "Healthy" areas decreased by 105.9 ha. The Natural Regeneration Index (IRN) revealed that 546.7 ha present medium regeneration, 362.1 ha low regeneration, and 120.9 ha no regeneration.

The supervised classification (Random Forest) combined with spectral indices determined that 403.5 ha (approximately 33% of the total analyzed area) are degraded, distributed as highly degraded mangrove (199.4 ha) and degraded mangrove (204.2 ha). Regenerating mangrove covers 288.6 ha, and healthy mangrove covers 546.6 ha. Overall classification accuracy was 87.3% with a Kappa coefficient of 0.84.

Six anthropogenic stressors were identified: solid waste disposal, untreated liquid waste disposal, estuary blockage, indiscriminate logging for charcoal, unplanned urban development, and agricultural and livestock activities. Natural stressors included hypersalinity, hurricane impacts, and pests such as the lepidopteran *Junonia genoveva* (affecting 80% of sampled areas), termites (*Nasutitermes nigriceps*), and fungal cankers (*Microthia* sp. on *Rhizophora mangle* (L.), *Eutypella* sp. on *Avicennia germinans* (L.)).

The integration of geoprocessing techniques (Sentinel-2 remote sensing, GIS, and field validation) allows for a precise diagnosis of post-disturbance mangrove condition. The established baseline (structure, cover, spectral indices, stressors) constitutes a predictive tool for land-use planning and prioritization of assisted restoration areas. These results directly support "Tarea Vida" (the Cuban State Plan for Confronting Climate Change), demonstrating that applied science can strengthen government decision-making for climate change adaptation in vulnerable coastal ecosystems.

Author Contributions

Conceptualization, Y.J.M.L. and I.d.l.C.M.C.; methodology, Y.J.M.L.; software, Y.J.M.L.; validation, G.d.l.C.R., and I.d.l.C.M.C.; formal analysis, G.d.l.C.R.; research, Y.J.M.L.; resources, I.d.l.C.M.C.; project management, I.d.l.C.M.C.; fundraising, Y.J.M.L. All authors have read and agreed to the published version of the manuscript.

Funding

The project "Management for the Conservation of Mangrove Forests in the Face of Climate Change in La Coloma, Pinar del Río" (Code: PT122PR002-010) was funded under Cuba's science and innovation programs. Main Funder: The budget was allocated through the Territorial Program for Natural Resources and Climate Change, coordinated by the Center for Environmental Research and Services (ECOVIDA) in Pinar del Río. Implementing Entity: The University of Pinar del Río "Hermanos Saiz Montes de Oca" was the institution responsible for managing the funds

and conducting the research. Support Framework: The project received methodological and strategic support from the international collaboration project "Mi Costa," which is externally funded by the Green Climate Fund.

Institutional Review Board Statement

Not applicable.

Informed Consent Statement

Not applicable.

Data Availability Statement

Data for this article are captured in the main text. Further information can be provided by the corresponding author on request.

Acknowledgments

The authors highlight the important support provided by the students of the Faculty of Forestry and Agricultural Sciences of the University of Pinar del Río and by the workers and specialists of flora and fauna of the community of La Coloma in the field work and data analysis carried out.

Conflicts of Interest

The authors declare no conflict of interest.

AI Use Statement

The authors declare that no artificial intelligence (AI) tools were used in the preparation of this manuscript.

Appendix A

Table A1. Geographic plane coordinates of each of the sampling units at the La Coloma intervention site.

Plot No.	Planar Coordinates (X, Y)
1	854196.029, 2465115.552
2	854329.709, 2465044.021
3	853984.955, 2464598.421
4	853898.180, 2464499.920
5	854219.481, 2464368.585
6	854711.987, 2464223.179
7	854484.496, 2464129.368
8	854829.250, 2463665.006
9	854034.205, 2463268.657
10	855267.814, 2463491.457
11	854709.642, 2463076.345
12	855511.722, 2462776.151
13	855373.351, 2461847.426
14	856212.956, 2461847.426
15	855910.417, 2460890.559
16	852929.909, 2463402.811
17	852984.885, 2463134.041
18	853192.571, 2462669.803
19	852642.814, 2463121.825
20	852624.489, 2462462.117
21	852172.467, 2462498.767
22	852001.432, 2461985.661
23	851360.049, 2462449.900
24	851573.843, 2461942.902
25	851158.472, 2461808.517
26	851189.014, 2461203.785
27	850663.691, 2461496.989

Table A1. *Cont.*

Plot No.	Planar Coordinates (X, Y)
28	850645.366, 2460794.522
29	849936.791, 2461179.352
30	850394.921, 2460434.126
31	850529.306, 2460061.513
32	849949.008, 2460763.980
33	853268.926, 2464013.652
34	853641.539, 2464242.717
35	853305.576, 2464407.644
36	853598.780, 2464819.961
37	853757.598, 2464926.858
38	853724.002, 2465400.260
39	853853.806, 2465853.809
40	853485.774, 2466122.579

References

1. Osland, M.J.; Feher, L.C.; Lopez-Portillo, J.; et al. Mangrove forests in a rapidly changing world: Global change impacts and conservation opportunities along the Gulf of Mexico coast. *Estuar. Coast. Shelf Sci.* **2018**, *214*, 120–140.
2. Green Climate Fund. Cuba's coastal communities fight climate change. Available online: https://www.greenclimate.fund/story/cubas-coastal-communities-fight-climate-change (accessed on 28 May 2025).
3. Milián Cabrera, I.C.; Muñoz Labrador, Y.J.; Rodríguez Crespo, G.C.; et al. *Management for the Conservation of the Mangrove Forest in the Face of Climate Change in La Coloma, Pinar del Río (Final Scientific-Technical Report of Project PT122PR002-10)*; University of Pinar del Río: Pinar del Río, Cuba, 2023.
4. Orjuela Rojas, A.M.; Villamil, C.A.; Sanjuan Muñoz, A. Extension and structure of mangrove forests in the Baja Guajira, Colombian Caribbean. *Bol. Invest. Mar. Cost.* **2011**, *40*, 357–376. (in Spanish)
5. Ellison, J. *Manual for Mangrove Monitoring in the Pacific Islands Region*; Secretariat of the Pacific Regional Environment Programme (SPREP): Apia, Samoa, 2012.
6. Muñoz Labrador, Y.J.; Milián Cabrera, I.C. Spatiotemporality in studies of vegetation and land use change. *Avances* **2023**, *25*, 599–622.
7. Climate-Data.org. Climate: Pinar del Río. Available online: https://en.climate-data.org/north-america/cuba/pinar-del-rio-1013/ (accessed on 28 May 2025).
8. O'Connell, J.L.; Castaneda-Moya, E.; Rivera-Monroy, V.H. Community-based mangrove restoration following a catastrophic hurricane in The Bahamas. *Wetl. Ecol. Manag.* **2025**, *33*, 46.
9. Fonds Français pour l'Environnement Mondial (FFEM). Restoring mangrove ecosystems in the Caribbean. Available online:https://www.ffem.fr/en/projects/restoring-mangrove-ecosystems-caribbean (accessed on 28 May 2025).
10. Wang, D.; Wan, B.; Liu, J.; et al. Estimating the growing stock of mangrove forests using multi-scale remote sensing. *Int. J. Appl. Earth Obs. Geoinf.* **2022**, *112*, 102915.
11. Caribbean Biodiversity Fund. Community-based coastal remediation in the insular Caribbean's two largest nations: Cuba and the Dominican Republic. Available online: https://caribbeanbiodiversityfund.org/project/community-based-coastal-remediation-in-the-insular-caribbeans-two-largest-nations-cuba-and-the-dominican-republic/ (accessed on 28 May 2025).
12. Fernández Martínez, F.R.; Muñoz Labrador, Y.J.; Milián Cabrera, I.C.; et al. Symptoms, signs and incidences of insects and phytopathogens associated with mangrove species. *Cuban J. For. Sci.* **2025**, *13*, e863.
13. Valdés Ramos, J.R.; Alonso Torrens, Y.; Hernández González, S.; et al. Richness and abundance of the assemblage of aquatic birds associated with mangroves of the Coloma-Las Canas sector. *Cuban J. For. Sci.* **2025**, *13*, e862.
14. Capote Fuentes, R.T. Resilience of Mangroves on the South Coast of Havana Province, Cuba. PhD Thesis, Rheinische Friedrich-Wilhelms-Universität Bonn, Bonn, Germany, 2007.
15. Cruz Portorreal, Y. Methodological Framework for Climate Change Mitigation Initiatives through Carbon Sequestration in Mangroves in Cuba. PhD Thesis, Universiteit Hasselt, Hasselt, Belgium, 2024.
16. Valero-Jorge, A.; González-Lozano, R.; González-De Zayas, R.; et al. An innovative tool for monitoring mangrove forest dynamics in Cuba using remote sensing and WebGIS technologies: SIGMEM. *Remote Sens.* **2024**,

16, 3802.
17. Cruz-Portorreal, Y.; Reynaldo, I.; Olivera, N.; et al. Mangrove forests dynamics in Havana, Cuba: responses to natural hazards and anthropogenic influence. In Proceedings of the General Assembly 2023 of the European Geosciences Union, Vienna, Austria, 24–28 April 2023.
18. Rodríguez-Rodríguez, J.A.; Mancera-Pineda, J.E.; Taillardat, P. Mangrove restoration in the Caribbean: challenges and opportunities. *Restor. Ecol.* **2022**, *30*, e13568.
19. Hernández-Ramírez, A.M.; Leal, M.; Clark, J.S.; et al. Coastal wetland restoration through nature-based solutions: The case of mangroves in Cuba. *Blue Carbon J.* **2024**, *1*, 89–104.
20. Rastandeh, A.; Brown, M.; Pedersen Zari, M. A review of the role of vegetation in ecosystem-based adaptation to climate change in coastal cities. *Nature-Based Solut.* **2023**, *4*, 100082.
21. Osorio, J.A.; Crous, C.J.; Wingfield, M.J. An assessment of mangrove diseases and pests in South Africa. *Forestry* **2017**, *90*, 343–358.
22. QGIS Development Team. *QGIS Geographic Information System V.3.24*; Open Source Geospatial Foundation: Beaverton, OR, USA, 2022.
23. Congedo, L. Semi-Automatic Classification Plugin: A Python tool for the download and processing of remote sensing images in QGIS. *J. Open Source Softw.* **2021**, *6*, 3172.
24. Campbell, J.B.; Wynne, R.H.; Thomas, V.A. *Introduction to Remote Sensing*, 6th ed.; The Guilford Press: New York, NY, USA, 2023.
25. Pettorelli, N. *The Normalized Difference Vegetation Index*; Oxford University Press: Oxford, UK, 2021.
26. Wang, Z.; Zhang, Y.; Li, F.; et al. Regional mangrove vegetation carbon stocks predicted integrating UAV-LiDAR and satellite data. *J. Environ. Manage.* **2024**, *366*, 122101.
27. Rouse, J.W.; Haas, R.H.; Schell, J.A.; et al. *Monitoring Vegetation Systems in the Great Plains with ERTS*; Nasa Special Publication: Washington, DC, USA, 1974; pp. 309–317.
28. Baloloy, A.B.; Blanco, A.C.; Candido, A.S.; et al. Mangrove species-level mapping using Sentinel-2 imagery and Google Earth Engine. *ISPRS Int. J. Geo-Inf.* **2020**, *9*, 556.
29. Jiang, C.; Ryu, Y.; Fang, H.; et al. Inconsistencies of interannual variability and trends in long-term satellite leaf area index products. *Glob. Change Biol.* **2017**, *23*, 4133–4146.
30. Jin, H.; Li, A.; Wang, J.; et al. Improvement of split-window algorithm for land surface temperature retrieval from Sentinel-3 SLSTR data. *ISPRS J. Photogramm. Remote Sens.* **2022**, *179*, 58–72.
31. Yan, Z.; Wang, W.; Chen, L. Physiological responses of mangroves to high salinity: A meta-analysis. *Mar. Environ. Res.* **2023**, *183*, 105812.
32. Gao, B.C. NDWI—A normalized difference water index for remote sensing of vegetation liquid water from space. *Remote Sens. Environ.* **1996**, *58*, 257–266.
33. Pham, T.D.; Yokoya, N.; Bui, D.T.; et al. Remote sensing approaches for monitoring mangrove species, structure, and biomass: Opportunities and challenges. *Remote Sens.* **2019**, *11*, 230.
34. Spalding, M.; Kainuma, M.; Collins, L. *World Atlas of Mangroves*; Routledge: London, UK, 2010.
35. Curtis, J.T.; McIntosh, R.P. An upland forest continuum in the prairie-forest border region of Wisconsin. *Ecology* **1951**, *32*, 476–496.
36. McAleece, N.; Gage, J.D.; Lambshead, P.J.; et al. *Biodiversity Professional V.2*; The Natural History Museum: London, UK, 1997.
37. Hammer, Ø.; Harper, D.A.T.; Ryan, P.D. PAST: Paleontological statistics software package for education and data analysis. *Palaeontol. Electron.* **2001**, *4*, 9.
38. Bravo, S.; Saura, S. Stability and change in Mediterranean landscapes. *Landsc. Ecol.* **2018**, *33*, 245–260.
39. Puyravaud, J.P. Standardizing the calculation of the annual rate of deforestation. *For. Ecol. Manag.* **2003**, *177*, 593–596.
40. Congalton, R.G.; Green, K. *Assessing the Accuracy of Remotely Sensed Data: Principles and Practices*, 3rd ed.; CRC Press: Boca Raton, FL, USA, 2019.
41. Landis, J.R.; Koch, G.G. The measurement of observer agreement for categorical data. *Biometrics* **1977**, *33*, 159–174.
42. R Core Team. *R: A Language and Environment for Statistical Computing V.4.2*; R Foundation for Statistical Computing: Vienna, Austria, 2022.
43. Alarcón Borges, R.Y.; Pérez Montero, O.; Barragán Muñoz, J.M.; et al. Institutional frameworks and strategies for implementing the socio-ecosystemic approach to coastal marine governance in Cuba. *Sustainability* **2025**, *17*, 4770.
44. Báez-Santamaría, J.; Flores-Cárdenas, F.; Herrera-Silveira, J.A. Monitoring detailed mangrove hurricane dam-

age and early recovery using UAV-based digital surface models. *J. Environ. Manage.* **2022**, *320*, 115837.
45. Gervacio Jiménez, H.; Castillo Elías, B.; Villerías Salinas, S. Diagnosis of mangrove areas affected by Hurricane Otis: Proposal for ecological restoration. In *Hurricane Otis in Acapulco, Guerrero: Socioeconomic and Environmental Vulnerability to the Impacts of the Hydrometeorological Phenomenon*; Comunicación Científica: Mexico City, Mexico, 2025, pp. 45–75. (in Spanish)
46. O'Connell, J.L.; Castaneda-Moya, E.; Rivera-Monroy, V.H.; et al. Multiple factors explain species-specific regeneration of mangrove seedlings and saplings following a major hurricane. *Ecosphere* **2025**, *16*, e70298.
47. Santiago-Valentín, E. Survival and Growth of Rhizophora mangle Propagules Deposited in a Coastal Dry Forest by Hurricane Maria. PhD Thesis, University of Puerto Rico, Río Piedras, Puerto Rico, 2022.
48. Zhang, Y.; Smith, T.J. Restoration enhances carbon storage in mangroves after hurricane impacts. *Front. Mar. Sci.* **2026**, *13*, 1722651.
49. Herrera Silveira, J.A.; Teutli Hernandez, C.; Secaira Fajardo, F.; et al. *Hurricane Damages to Mangrove Forests and Post-Storm Restoration Techniques and Costs*; The Nature Conservancy: Arlington, VA, USA, 2022.
50. Xia, Q.; Gao, Z.; Li, Z.; et al. Mangrove biomass estimation using Sentinel-2 and Sentinel-1 data in a subtropical mangrove forest. *Remote Sens.* **2020**, *12*, 3694.
51. Wang, L.; Jia, M.; Yin, D.; et al. A review of remote sensing for mangrove forests: 1956–2018. *Remote Sens. Environ.* **2020**, *237*, 111541.
52. Toosi, N.B.; Fakheran, S.; Some'e, B.S. Mangrove ecosystem health assessment using the Normalized Difference Vegetation Index (NDVI) and Sentinel-2 imagery. *Mar. Pollut. Bull.* **2022**, *174*, 113280.
53. Ghorbanian, A.; Mohammadzadeh, A.; Jamali, S.; et al. Mangrove ecosystem mapping using Sentinel-1 and Sentinel-2 data and a Google Earth Engine-based cloud computing platform. *Remote Sens. Appl. Soc. Environ.* **2021**, *21*, 100445.
54. Navarro, A.; Young, M.; Becek, K.; et al. Evaluation of Sentinel-2 and Landsat 8 data for mangrove mapping and carbon stock estimation. *Remote Sens.* **2020**, *12*, 3110.
55. Xolalpa-Aroche, G.A.; Flores-Sánchez, D. Structure and composition of mangroves in Cuyutlán lagoon, Colima, Mexico. *Rev. Biol. Trop.* **2021**, *69*, 850–864.
56. Zacarias, D.A.; Williams, S.; Lovelock, C.E. Mangrove restoration under shifted baselines and future uncertainty. *Restor. Ecol.* **2022**, *30*, e13618.
57. Ferreira, A.C.; Lacerda, L.D. Mangroves' response to environmental changes: A review of the last 10 years of research in Brazil. *An. Acad. Bras. Cienc.* **2023**, *95*, e20220255.
58. Friess, D.A.; Howard, J.; Huxham, M.; et al. Building a bridge between mangrove science and policy. *Ocean Coast. Manag.* **2022**, *223*, 106154.
59. Muñoz Labrador, Y.J.; Milián Cabrera, I.C.; Rodríguez Crespo, G.C.; et al. Dynamics of mangrove cover southwest of Pinar del Río, Cuba. *Avances* **2024**, *26*, 315–333.
60. Lagomasino, D.; Fatoyinbo, T.; Castañeda-Moya, E.; et al. Storm surge and ponding explain mangrove dieback in southwest Florida after Hurricane Irma. *Nat. Commun.* **2021**, *12*, 1–12.
61. Adame, M.F.; Connolly, R.M.; Turschwell, M.P.; et al. Future carbon emissions from global mangrove loss. *Glob. Change Biol.* **2021**, *27*, 2856–2866.
62. Su, J.; Friess, D.A.; Gasola, S. Mangrove restoration outcomes and their carbon sequestration potential. *Curr. Biol.* **2022**, *32*, R1230–R1231.
63. Zhang, K.; Liu, H.; Li, Y.; et al. The role of mangroves in attenuating storm surges: A case study of Hurricane Wilma. *Estuar. Coast. Shelf Sci.* **2020**, *244*, 106922.
64. Dale, P.E.; Knight, J.M.; Dwyer, P.G. Mangrove rehabilitation: A review of hydrological restoration. *Wetl. Ecol. Manag.* **2021**, *29*, 1–17.
65. Menéndez Carrera, L.; Guzmán Menéndez, J.M.; Planos Gutiérrez, E.O.; et al. Dynamics of mangrove cover in the province of Pinar del Río, Cuba: Period 2000–2020. *Cuban J. For. Sci.* **2022**, *10*, 185–201.
66. Capote-Fuentes, R.T.; Pérez-Martínez, R. Application of vegetation indices for monitoring resilience in mangrove ecosystems to extreme events in western Cuba. *Ser. Oceanol.* **2023**, *18*, 45–62.